Multi-Spectral Imaging Ellipsometer for Fast, In-Situ Monitoring of Monolayer Film Deposition

Contract No. DAAG55-98-C-0024
Period of performance: 12/01/97 to 05/31/98

Final Report

Presented to :

Army Research Office
P.O. Box 12211
Research Triangle Park, NC 27709-2211

Technical Monitor :

Dr. Jack Rowe
(919) 549-4332

Presented by :

Physical Optics Corporation
Research & Development Division
2520 West 237th Street
Torrance, California 90505

Principal Investigator :

Lothar U. Kempen, Ph.D.
(310) 530-7130

May 31, 1998

PREFACE

This final report was prepared by Physical Optics Corporation, 2520 W. 237th Street, Torrance, CA 90505, under Contract No. DAAG55-98-C-0024, for the U.S. Army Research Office, PO Box 12211, Research Triangle Park, North Carolina 27709-2211.

The report describes the design and realization of an imaging ellipsometer for the fast characterization of very thin amorphous films, and the results of measurements on test samples, demonstrating the feasibility of our approach. We furthermore established a software algorithm for evaluating the film parameters from the data yielded by our system, and employed this algorithm to a large number of measurements in order to check the stability of the mathematical model.

The principal investigator and author of this report wishes to acknowledge the technical support of Dr. Srivatsa V. Rao and Mr. Peter Low at Physical Optics Corporation. The author also wishes to thank Dr. Jack Rowe of the Army Research Office for his supervision of the project.

1.0 INTRODUCTION

1.1 Objectives

The goal of the Phase I project was to demonstrate the feasibility of mapping the thickness of amorphous layers in the monolayer thickness range using an imaging ellipsometer setup. Phase I addressed three objectives:

Objective 1. *Create a system design capable of producing a stable, highly parallel, polarized beam from an incandescent source, such as a xenon arc lamp. Design a detection system to acquire ellipsometer intensities. In the system design, take into account the specific requirements for attaching the setup to a vacuum reaction chamber.*

POC successfully met this objective by establishing an illumination system using a 75W short arc lamp combined with a confocal lens array using a 200 μm pinhole and a 10 nm wide interference bandpass filter. The resulting light beam of about 1" radius had a divergence angle smaller than 1.3 mrad and a beam uniformity of less than 15% intensity variation across the beam cross-section. A detection system was set up using a commercial CCD camera and a high-resolution framegrabber card in a PC. To achieve highest sensitivities, we also employed a thermoelectrically cooled CCD camera in our test setup, thus reducing the thermal noise to a fraction of the noise compared to the standard video camera.

Objective 2. *Set up a fast data acquisition system for pixel-synchronous, fast readout of the camera. Calculate the relationship of the reflected beam properties with the film parameters and write software to evaluate the film parameters on-line.*

Using a fast framegrabber board for the PCI bus of a PC (Mutech MV 1000), POC established a high-resolution (10 bit) image acquisition system. We created various software algorithms using the MatLab™ development platform, based on the Jones matrix calculus, in order to relate the measurement results from the ellipsometric system to film thickness and refractive index values. We theoretically investigated the dependence of the measurement results upon different parameter variations, allowing us to identify the most critical measurement parameters. The results of these studies will help to improve the system in Phase II of the project.

Objective 3. Demonstrate prototype performance by monitoring amorphous film growth in a vacuum reaction chamber. Demonstrate the imaging capabilities of the measurement system by evaluating unevenly coated substrates.

In order to investigate the system performance, we checked the ellipsometer setup with various test structures. Using native oxide layers on silicon wafers, commercial ellipsometer check samples, and specifically prepared silicon surfaces partially covered with silane layers, we verified the capability of the system to detect and measure extremely thin amorphous layers.

1.2 Background

The deposition of extremely thin films is playing an increasingly important role in a wide range of modern scientific and technological applications. Many recent developments in semiconductor sciences make use of physical effects observed solely in very thin layers, such as in quantum films or quantum dots; others utilize a large number of thin films of alternating properties as specifically tailored crystal lattices (superlattices) or as extended optical gratings, like in vertical-cavity surface emitting lasers (VCSELs). The deposition of crystalline monolayers has become established due to advanced epitaxial growth methods, such as molecular beam epitaxy (MBE), and because of advanced characterization methods, such as Reflectance Anisotropy Spectroscopy (RAS) [1]. RAS, however, uses the reflectance anisotropy caused by the orientation of crystal axes with light at normal incidence and has so far not been suitable for amorphous layers. An increasing number of applications require the controlled deposition of amorphous monolayers. Although current technologies can deposit such thin layers, established systems for deposition control, such as thin-layer interferometry, cannot resolve thickness changes in the required range of 1/1000 of a wavelength. Minimum detectable thicknesses of SiO_2 layers as thin as 0.36 Å (0.1 monolayer) have been reported using x-ray fluorescence (XRF) [2], but this technique is very difficult to adapt to a reaction chamber for in-situ measurements during the coating process. Additionally, for the formation of extremely thin layers, the uniformity of the coating process becomes a crucial parameter, requiring online information about the film thickness in various locations on the surface of the substrate.

1.3 Scope/Approach

The concept followed by POC to address the shortcomings of the existing approaches makes use of imaging ellipsometry, a fast, very precise method for analyzing surface topography without scanning devices. While resolution in the 5 Å range has been demonstrated using this technology [3], its accuracy can be further increased by performing a multi-wavelength analysis. This leads, in effect, to the simultaneous measurement of a vast number (>200,000) of parallel points, all with the superior resolution of spectroscopic ellipsometry. The device can thus be used to monitor the coating process and to test coated samples; it can be used in laboratory environments and in manufacturing.

The system POC proposed consists of an illumination unit and a detection system, connected to sapphire ports of the deposition reaction chamber (see Figure 1-1). The thickness of the deposited layer is monitored over the entire substrate surface with a frame rate of less than one second, which is sufficient for online control and for kinetic studies of the deposition process. Performing the measurements in a number of narrow wavelength bands improves the signal-to-noise ratio, which could otherwise suffer from the broadband light emission of the RF plasma employed in many current deposition processes, such as plasma enhanced chemical vapor deposition (PECVD) [3].

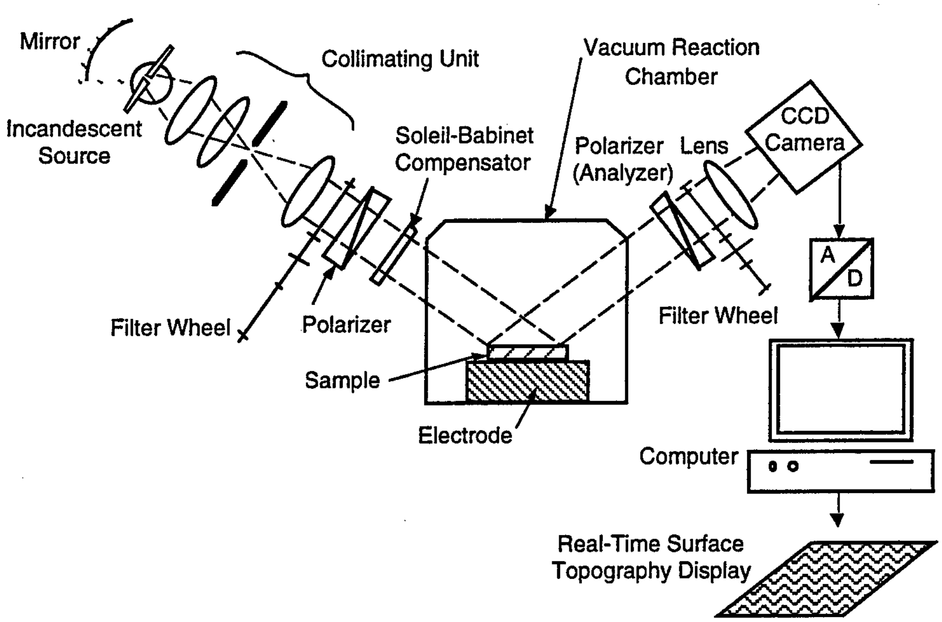

Figure 1-1
Multi-spectral imaging ellipsometer for in-situ monitoring of monolayer deposition.

The use of visible light to perform the measurement has several advantages compared to other approaches. Access to the vacuum reaction chamber in typical deposition units is through transparent windows, usually made from sapphire, to provide high-temperature and radiation stability. Adapting an X-ray source to perform a similar measurement (as required for the X-ray photoelectron spectroscopy method) would require major system changes, and could produce other problems, such as interference with the radiation from the plasma discharge and the drawbacks of single-point measurement. Additionally, POC's system consists entirely of standard, off-the-shelf components, making it a cost-effective solution.

In the course of the Phase I research effort, POC was able to achieve:

- Successful creation of a highly parallel, highly uniform, quasi-monochromatic illumination source for illuminating the test sample.

- Establishment of a high-precision large-diameter polarizing optical signal train in order to obtain tight control upon the polarization state of the light falling onto the sample, and to precisely analyze the polarization state of the reflected light.

- Setup of a low-noise, high-resolution detection camera combined with a fast framegrabber system with high quantization depth (10 bit), allowing for rapid acquisition of the radiation distribution emerging from the imaging ellipsometer system.

- Successful determination of film thickness both in SiO_2 and Si_3N_4 layers on check samples used for calibrating commercial ellipsometers.

- Creation of test samples containing patterned monolayers on a silicon chip for testing the imaging capabilities of the instrument.

- Establishment of a theoretical model of the polarization state of light propagating through the system using an extended Jones matrix formalism, which takes into account the non-ideal properties of the optical components.

- Creation and implementation into programs of numerous software algorithms for relating the measurements to film parameters using the mathematical model

mentioned above. The programs were established employing the Matlab platform, which also allowed predictions on the accuracy of the measurement.

- Investigation of the effect of slight inaccuracies in the measurement parameters on the film thickness determination, which allowed the identification of the most critical parameters and ensured their precision in the measurement process.

Thus, POC has achieved the proposed goals by determining the thickness of extremely thin layers on a silicon substrate. The results achieved clearly lay the foundation for the Phase II development of a multi-spectral imaging ellipsometer for the fast, in-situ monitoring of monolayer film deposition.

2.0 DESIGN OF OPTICAL SYSTEM

2.1 Illumination System Layout

The ellipsometric measurement of an extended area imposes strong requirements on the illuminating system. The light being directed onto the sample must meet the following parameters:

- Highly parallel illumination beam
- Well-defined, stable angle of incidence
- Narrow spectral bandwidth to maximize polarization contrast; choice of various wavelengths
- Well-controlled polarization state
- High intensity for maximizing signal-to-noise ratio on the detector system

An incandescent source, combined with an optical interference bandpass filter (for selecting a narrow section of the emission spectrum), was chosen for the illumination system. This permits choosing between various wavelengths by simply exchanging the filter. The filter is simpler, and has a smaller spectral transmission variation across the beam area, than a grating-based spectrograph. The higher bandwidth illumination light avoids the formation of interference speckle patterns in the image plane. These patterns, common to laser sources, cannot be interpreted by the detection system.

The setup of the illumination system is depicted in Figure 2-1. Light from an incandescent source passes through a condenser lens which collimates the light from the emitting area. It is then focused by a second lens onto a pinhole that is also in the focal point of a third lens. Since only the parallel light falling onto the second lens is focused exactly onto the pinhole, all the nonparallel light is discarded, so that a parallel beam emerges from Lens 3. The size of the pinhole, generally chosen as a trade-off between parallelism and intensity, was evaluated experimentally; the diameter is usually in the range of several hundred microns (see Section 2.2).

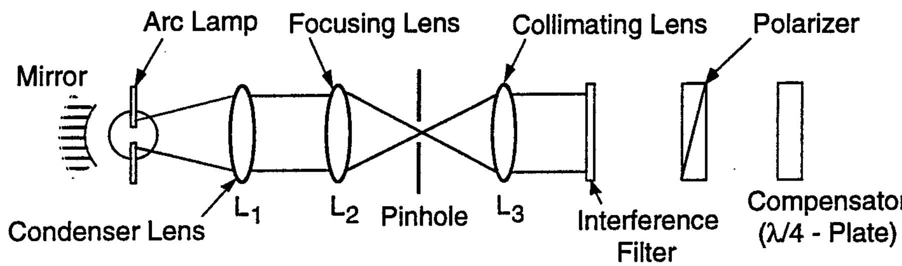

Figure 2-1
Design of the illumination system.

An important parameter for effectively focusing the beam is the size of the emitting area in the lamp. A study of commercially available light sources showed that short arc lamps produce the highest energy flux per unit of emitting area. Table 2-1 shows a comparison between different lamp types (xenon arc and quartz tungsten halogen) of various specified operating powers. The table is based on data from a lamp manufacturer's catalog [4].

Table 2-1. Comparison of Different Lamp Types with Respect to Emitted Light Energy Per Arc Area

Lamp type	Emitting area [mm^2]	Intensity of strongest peak in 0.5 m distance [$mW/m^2/nm$]	Intensity normalized to emitting area [$mW/m^2/nm/mm^2$]
75 W Xe	0.125	70	560
150 W Xe	1.1	200	182
300 W Xe	1.68	500	298
500 W Xe	3	1000	333
10 W QTH	1.14	29	2.5
50 W QTH	5.28	10	1.9

A high-power lamp produces intense light with a large arc; in the described system this light would be lost at the pinhole. Choosing a high-power lamp would effectively decrease the intensity of the collimated light beam; a low-power lamp has higher power density and thus is best suited for focusing onto a pinhole and creating a highly collimated beam.

We decided to employ a 75 W Xenon short arc lamp for the system. The lamp, with an appropriate housing and a built-in ignitor, and a stabilized power supply were ordered from Oriel Corporation (Stratford, CT). The housing incorporates a condenser lens that provides initial beam collimation for the light being directed into the subsequent collimating system.

2.2 Setup and Test of Illumination System

The illumination system was set up and tested. Various system parameters were investigated to evaluate the setup best suited for yielding a highly parallel, uniformly illuminated spot.

The components of the illumination system were installed according to Figure 2-1. Figure 2-2 shows a photograph of the system. In choosing the pinhole size, consideration was given to the trade-off between beam parallelism and signal sensitivity. The divergence angle of the beam is dependent on the size of the pinhole used; a smaller pinhole creates a better collimated beam. However, a very small pinhole leads to very low signal intensity, which ultimately affects the signal-to-noise behavior of the system. The interference filter produces a quasi-monochromatic beam; the neutral density filter is used during the camera measurement to adapt the beam intensity to the dynamic range of the camera.

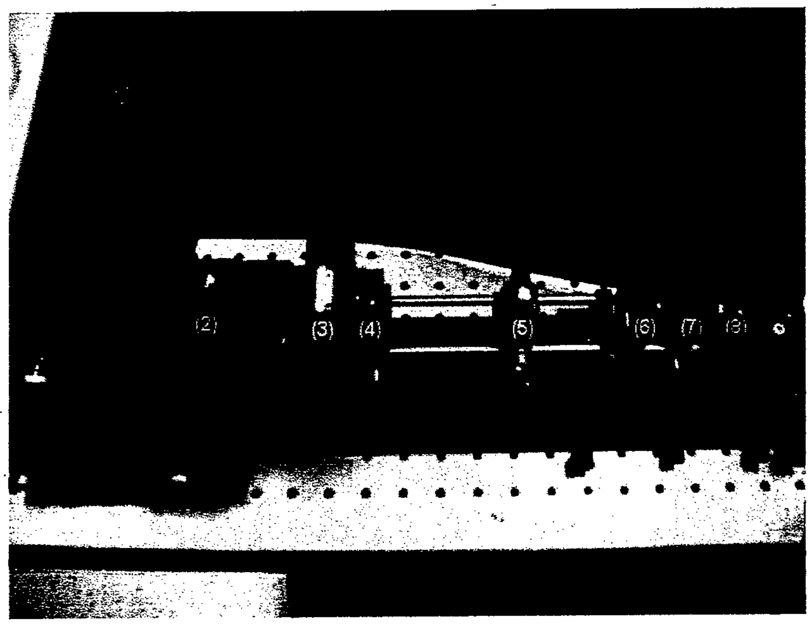

Figure 2-2
Setup of the collimation system: (1) Xenon short arc lamp (2) Condenser (3) Holder for diffuser or other elements (4) Lens 1 (5) Pinhole in xy-stage (6) Lens 2 (7) Interference bandpass filter (8) Adjustable iris.

A number of different pinhole sizes were tested for suitability. In some of the experiments, a diffuser was introduced into the beam path between the condenser lens and the first focusing lens. This component -- a commercial product manufactured by POC -- provides a more uniform intensity distribution across the beam profile while maintaining a defined angular range for the light emerging from the device. It was expected that this would allow larger pinholes to be employed for the same beam uniformity. The disadvantage of this additional component is its negative influence upon the focusing behavior of the first focusing lens, thus reducing the amount of light passing through the pinhole. For the experiments, a diffuser with a specified angular divergence of 0.3° was utilized.

Additionally, an optical interference filter -- with a 10 nm transmission band around 633 nm (OptoSigma Corp.) -- was placed into the beam path to provide quasi-monochromatic illumination, as required for the ellipsometric measurements. The filter's transmission curve is shown in Figure 2-3. Since this element is an essential part of the ultimate system, its influence upon the divergence and uniformity properties of the beam had to be determined.

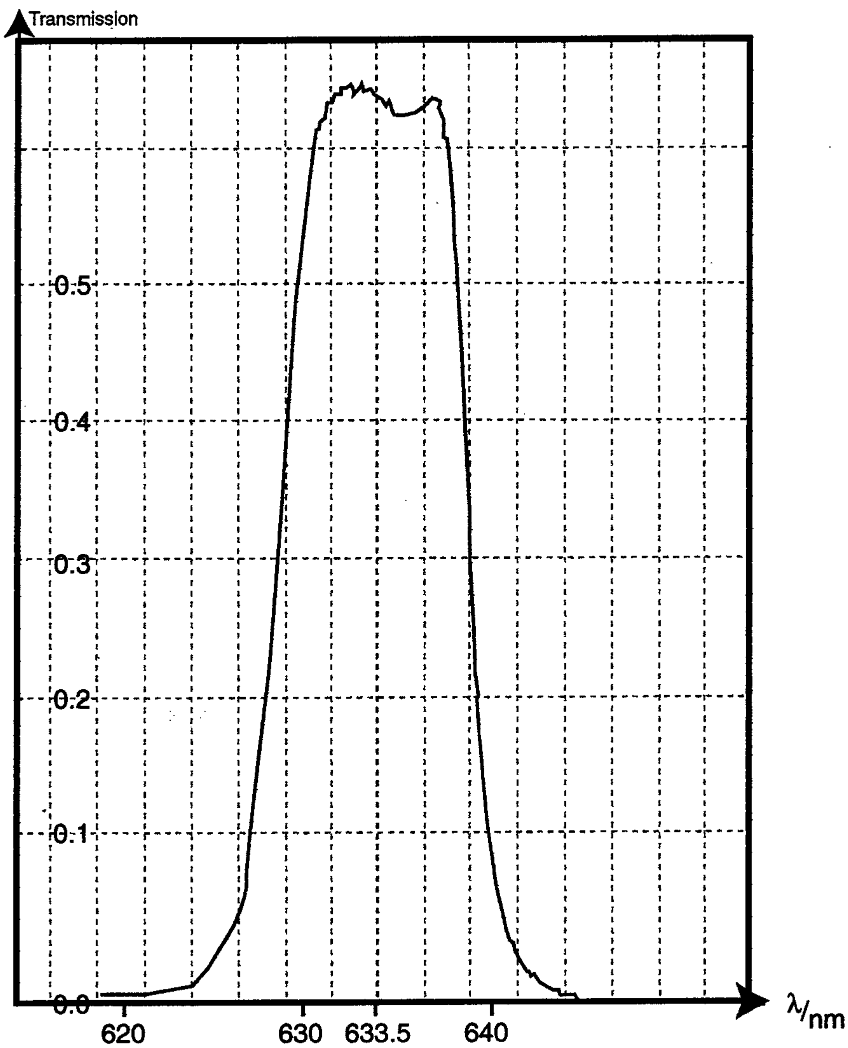

Figure 2-3
Transmission spectrum of the interference bandpass filter.

To determine the beam divergence angle, the beam diameter was measured at different locations along a propagation distance of about 3 meters. For this purpose, a projection screen was placed in the beam path at each location; the beam diameter was visibly determined using a caliper. The beam divergence angle α was subsequently calculated from the beam diameters d_1 and d_2 at the distance between the two locations, l, using the formula

$$\alpha = \arctan\frac{r_2 - r_1}{l} = \arctan\frac{d_2 - d_1}{2 \cdot l} \quad , \tag{2-1}$$

where r_1 and r_2 are the beam radii corresponding to the beam diameters d_1 and d_2, respectively.

The signal intensity was determined by placing an optical power meter (Newport Model 840) in the beam path. Using the calibration function for the large area detector (Newport Model 818-UV, $\lambda = 0.25$ - $1.1\ \mu m$), the power meter reading was calibrated for the wavelength of the incident light ($\lambda = 633$ nm).

Beam uniformity over the illuminated area is another important parameter for ensuring precise measurements. To measure beam uniformity, the image of the beam cross-section was acquired by a CCD camera positioned directly in the beam path. The beam intensity for each measurement was adapted to the dynamic range of the camera by placing appropriate neutral density filters in the beam path.

The experimental data from this measurement series is depicted in Figure 2-4 (without diffuser) and in Figure 2-5 (with diffuser) employing pinhole sizes of 200, 300 and 600 µm. The intensity pattern is color-coded, as shown in the figure legends. The intensity profile is shown in two mutually orthogonal cross-sections. For each measurement series, it can be clearly observed that when the pinhole size is increased, a spot of higher intensity forms in the center of the beam cross-section, thus degrading beam uniformity.

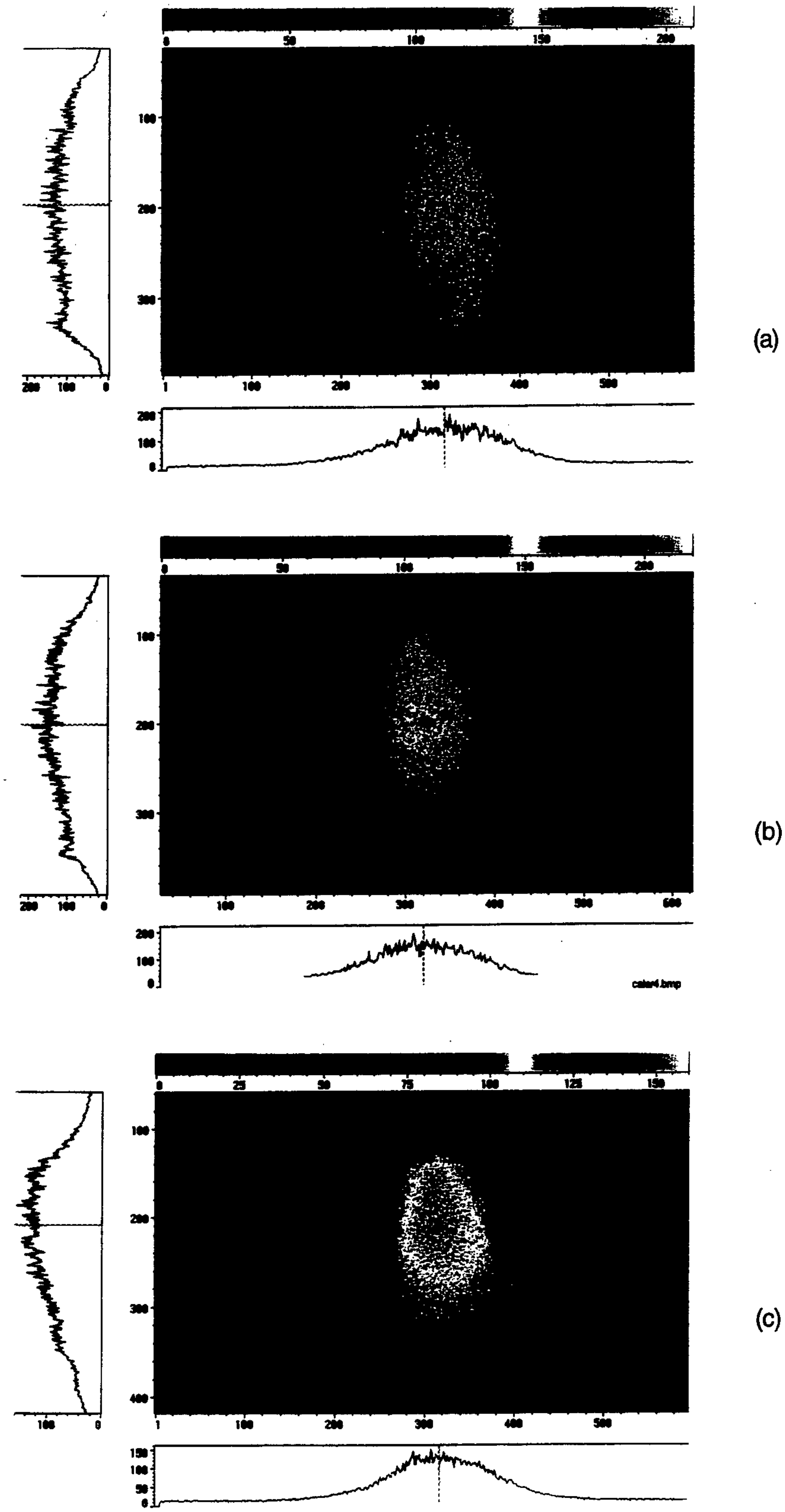

Figure 2-4
Beam intensity profiles for the illumination system without diffuser.
Pinhole sizes: (a) 200 μm, (b) 300 μm, (c) 600 μm.

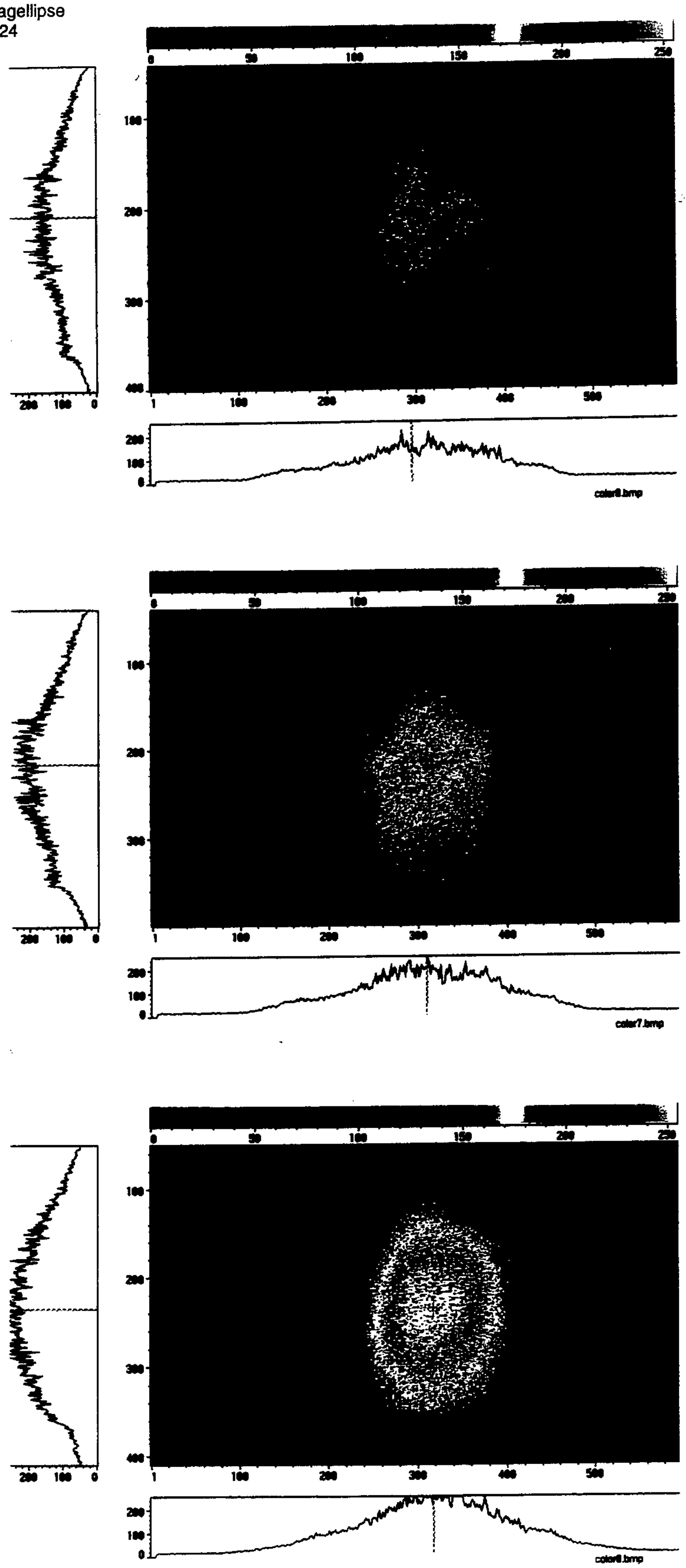

(a)

(b)

(c)

Figure 2-5
Beam intensity profiles for the illumination system with diffuser.
Pinhole Sizes: (a) 200 µm, (b) 300 µm, (c) 600 µm.

The data yielded by these measurements can be interpreted more conveniently by using a histogram of the beam intensities, as shown in Figure 2-6.

While the absolute value of the measured intensities is arbitrary (it is determined by the respective choice of neutral density filters), the graph shows varying distribution of intensity values for different pinhole sizes.

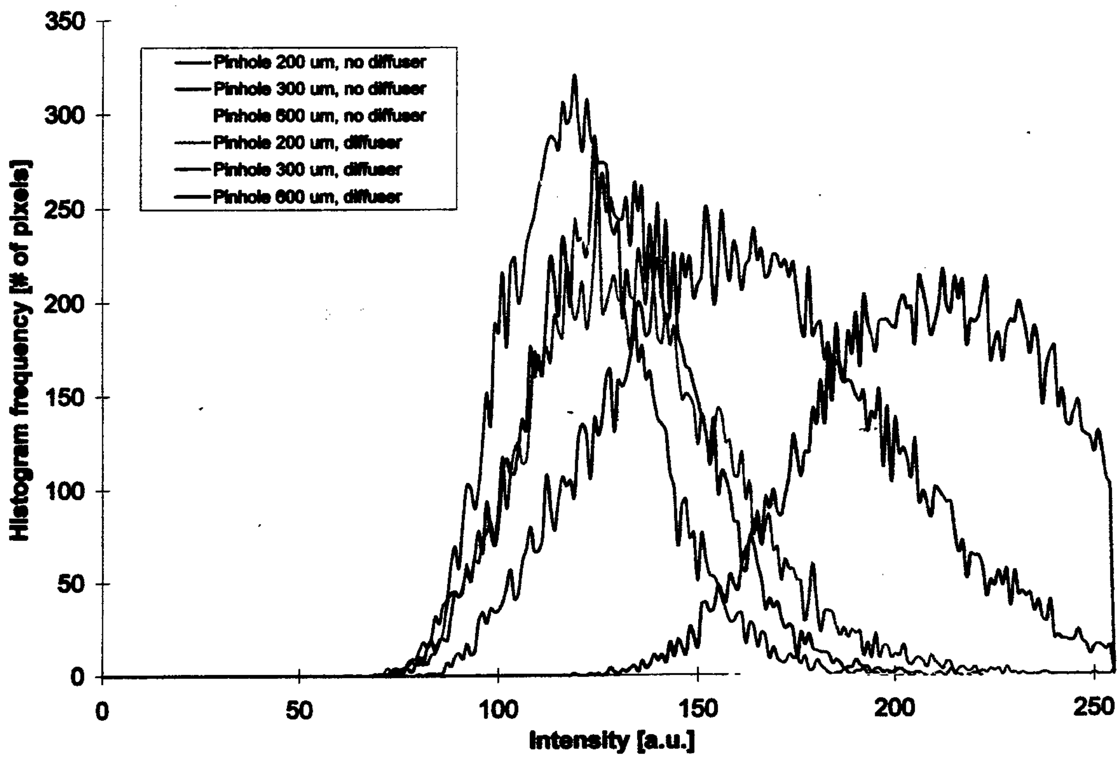

Figure 2-6
Intensity histogram for the beam cross-sections for different system parameters (compare to Figures 2-4 and 2-5).

Table 2-2 summarizes the results of the measurements performed with and without the diffuser, and employing pinholes with diameters of 200, 300 and 600 μm.

Table 2-2. Beam Properties of Light from the Illumination System under Varying Conditions

Diffuser	Pinhole size	Divergence angle	Rel. covariance	Signal intensity
no	200 µm	1.26 mrad	14.9 %	25.5 mW
no	300 µm	1.44 mrad	15.5 %	66 mW
no	600 µm	5.03 mrad	14.9 %	290 mW
yes	200 µm	0.65 mrad	18.6 %	2.4 mW
yes	300 µm	2.42 mrad	20.3 %	5.0 mW
yes	600 µm	4.84 mrad	12.7 %	21.7 mW

The table shows divergence angles between 1.3 and 5 millirad (0.07° to 0.29°) for different pinhole sizes without the diffuser. Introducing the diffuser into the beam path slightly improved the collimation (after realignment of the system), however, the signal levels are reduced by approximately a factor of ten. This significant loss in signal intensity made the diffuser unsuitable for the system. It also did not significantly improve the intensity variation across the beam profile, which can be judged by the relative covariance of the pixel intensities measured in the above described experiments. As a result of our testing, we decided to conduct our ellipsometric measurements with a pinhole diameter of 200 µm and no diffuser.

2.3 Setup of Polarization Components

Since the system required the use of an extended beam (about 1" diameter) for the investigation of the surface, the polarizers had to have a corresponding diameter. This restricted us to dichroic sheet polarizers, since devices based on birefringent crystals (Glan-Thompson / Glan-Taylor polarizers) are available at reasonable prices only up to clear apertures of 20 × 20 mm. The extinction ratio for the perpendicular polarization (40 dB) of the sheet polarizers was considered to be sufficient for our application. We therefore decided to order dichroic sheet polarizers with a diameter of 30 mm from Melles-Griot, Inc. The selected components have a specified extinction ratio of 10^{-4} and are virtually insensitive to changes in the angle of incidence.

For the Phase I investigations, we used the wavelength of the red HeNe laser (632.8 nm). We ordered a quarter-wavelength plate at this wavelength to convert linear polarization into circular polarization. Subsequently, the polarizing components were set up and tested. The system layout is depicted in Figure 2-7. Collimated and filtered light is directed through the system components

in the order shown: Polarizer-Compensator-Sample-Analyzer (PCSA). The linearly polarized light (emerging from the polarizer) passes through the compensator, a polished birefringent crystal, which introduces a spatial retardation of $\lambda/4$ between two orthogonal polarization components. When the compensator is placed at a 45° angle to the polarizer, the resulting light beam is circularly polarized; any other azimuth angle produces elliptically polarized light. This light is reflected by the measured sample, introducing additional changes in polarization characteristics for the specific film-substrate system. The reflected beam is directed through the "analyzer", the second linear polarizer in the system. In null ellipsometry, the polarizer-compensator setup is angularly adjusted to produce a beam with a specific elliptical polarization, such that the beam reflected from the sample is linearly polarized. This reflection can be totally blocked by the analyzer. The specific combination of azimuth angles that are required to produce this condition can be used to determine the composition of the investigated sample. When using an extended, quasi-monochromatic, highly parallel beam to illuminate the sample, the "null condition" can be fulfilled over the entire beam cross-section only when the sample surface is absolutely optically homogeneous. Any local deviation from this condition will result in a non-zero intensity emerging from that point of the sample. ***This is the "heart" of POC's novel technique: after adjusting the null condition on the sample surface while imaging the output intensity pattern with a camera, the measured image intensity yields information about the surface topography of the sample.***

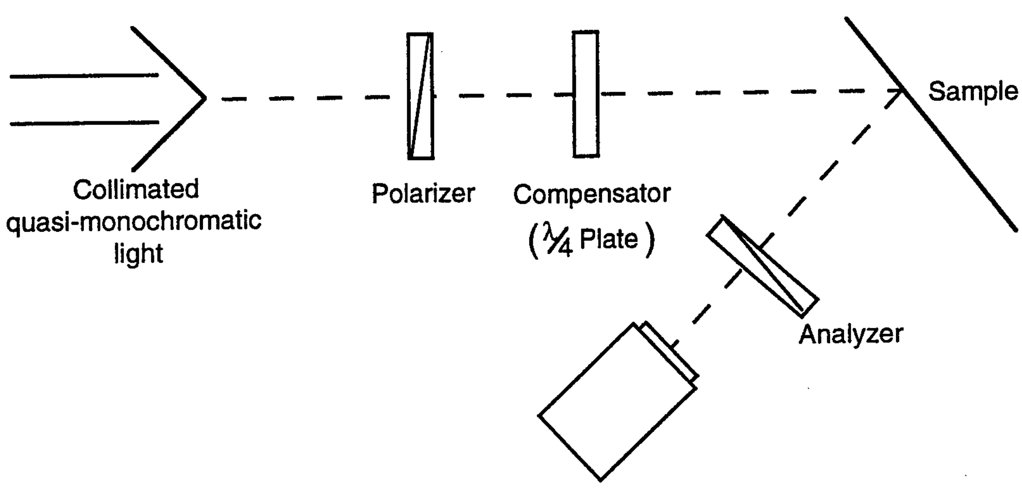

Figure 2-7
Layout of the polarization-controlling optical system.

The selected compensator is a multiple-order quartz wave plate with a retardation of $\lambda/4$ at 632.8 nm. Quartz plates show lower absorption, better homogeneity, and more precisely defined retardation than plates fabricated from mica, a birefringent crystal commonly used for lower-cost systems. The choice of a multiple-order plate requires a relatively precise control of the angle of incidence; the retardation value changes significantly with the angle (e.g., from +0.0023 λ at a 1° angle up to +0.235 λ at a 10° angle, calculated for a 1 mm thick quartz plate at 632.8 nm wavelength).

In a later stage of the project, we replaced this component with a liquid-crystal variable retardation plate. The variable plate enabled the system to operate at multiple wavelengths by adjusting the appropriate retardation according to the chosen wavelength. This component is a true zero-order retarder, so that the above described angular dependence of the retardation will be significantly reduced. The variable retardation plate was ordered from Meadowlark Optics Corp. (Frederick, CO). Since the lead time for this component was more than two months, we were only able to investigate multi-wavelength operation of the ellipsometer in the last stage of the Phase I project.

2.4 Adjustment of the Polarizing Components

The angular positions of the polarizing components in the ellipsometer have to be controlled precisely to obtain accurate measurements. The polarizers and the compensator have to be individually mounted in precision rotation stages, where their azimuth angle can be read from a vernier scale. The optical components and the stages were shipped separately and had to be assembled. The angular position of each component had to be adjusted with respect to the vernier scale before the setup could be used for measurements.

Both dichroic sheet polarizers were adjusted by employing a pre-adjusted Glan-Thompson polarizer, as depicted in Figure 2-8. The sheet polarizer was adjusted to minimize the light intensity measured by the optical power meter, i.e., to be in a crossed position with the Glan-Thompson polarizer. A helium-neon laser, which produces an intrinsically polarized beam, was used as a light source. The $\lambda/4$-waveplate was placed in front of the optical arrangement. The waveplate had not yet been adjusted, but its arbitrary azimuth position generally results in an elliptically polarized beam. Therefore, the intensity measurement was not influenced by the angular adjustment of the HeNe laser. Both polarizers to be used in the system were adjusted to the vernier scale of their rotation stages using this setup.

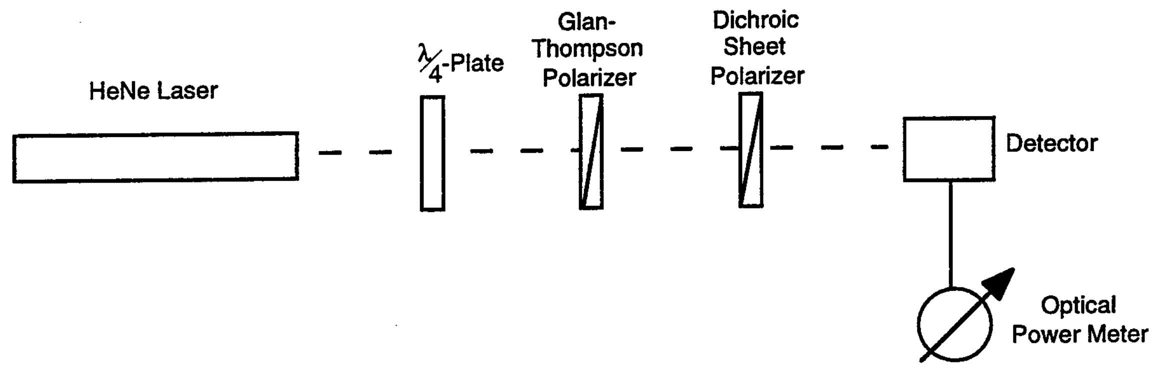

Figure 2-8
Setup for the azimuthal adjustment of the polarizers.

The arrangement in Figure 2-9 was used for calibrating the angular position of the compensator. The light from the HeNe laser passes through a beam splitter cube, a polarizer, and the $\lambda/4$ plate, and is subsequently reflected by a metallic mirror. The reflected light beam passes back through the compensator and polarizer and is separated into two beams in the beam splitter. One of the beams is directed into the detector of an optical power meter. (The other beam goes in the direction of the laser and is lost).

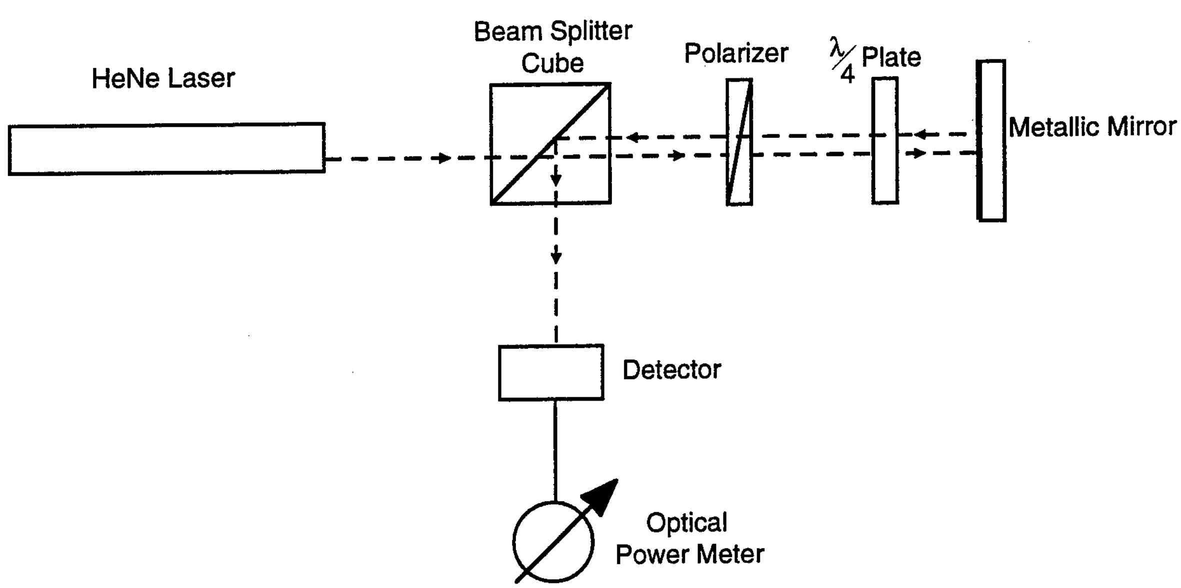

Figure 2-9
Setup for the azimuthal adjustment of the compensator.

When the compensator is adjusted at precisely 45° with respect to the polarizer, the light falling on the mirror is circularly polarized. The mirror reverses the parity of the circularly polarized light, so that the linearly polarized light emerging from the compensator on the reverse path is polarized in an orthogonal direction to the polarizer. Therefore, the compensator was precisely adjusted to 45° by minimizing the intensity measured by the optical power meter.

The adjusted components were integrated into the ellipsometer system shown in Figure 2-10. The collimated and filtered light from the xenon light source can quickly be interchanged with a HeNe beam that can be led into the beam path by flipping a mirror. This provides a convenient method for quickly testing system performance with a perfectly monochromatic and collimated beam. The sample holder is mounted on a precision rotation stage and can additionally be adjusted in two orthogonal directions by linear translation stages. The light reflected from the sample is directed through the analyzer to the camera, which is connected to the frame grabber board in the computer.

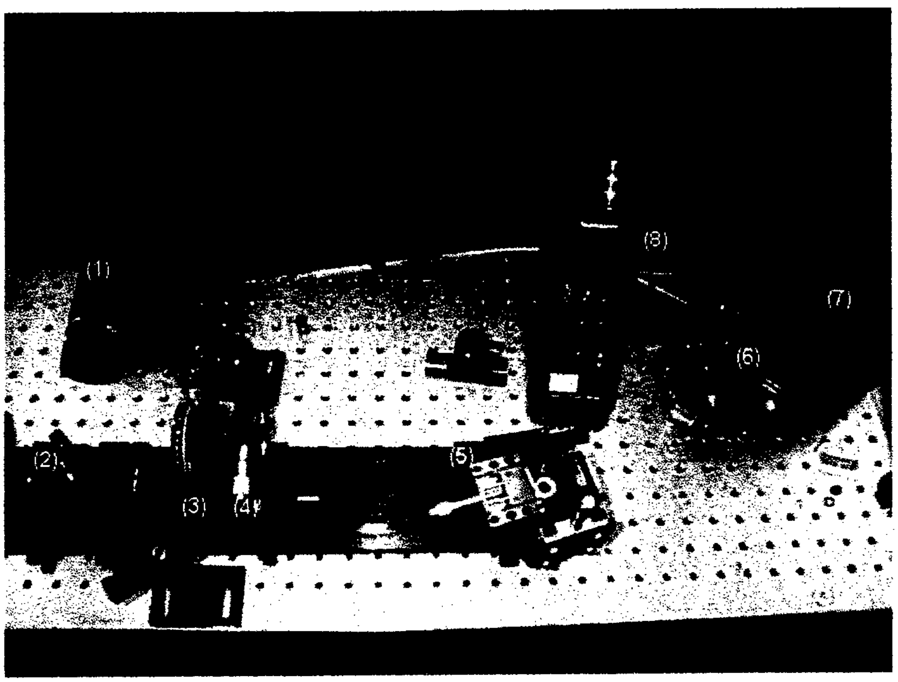

Figure 2-10
Ellipsometer setup in configuration for null ellipsometry: (1) HeNe Laser (2) Mirror (3) Polarizer (4) Compensator (5) Sample stage (6) Analyzer (7) Detector (8) Optical power meter.

2.5 Detection System Evaluation

A high-resolution monochrome camera was used for detecting the irradiation pattern reflected from the sample surface. The camera had to meet the following requirements:

- High sensitivity
- High signal-to-noise ratio
- External shutter adjustment
- Access to the pixel clock (to precisely synchronize the data acquisition).

These requirements are best fulfilled by a CCD camera designed for technical imaging. The following cameras were considered for this purpose:

Table 2-3. Properties of Commercially Available Camera Types

Manufacturer	Type #	Size/Resolution	Signal-to-Noise Ratio	Additional Features
Hitachi	KP-M3	1/3", 768 × 494	56 dB	Shutter speed 1/100..1/10,000 s
Sony	XC-73	1/3", 768 × 494	56 dB	Pixel clock output
Pulnix	TM-7 CN	1/2", 768 × 494	50 dB	Pixel clock output
Kodak	Megaplus 1.6i	0.54" × 0.36", 1534 × 1024	60.2 dB	Digital output

The first three cameras in the table incorporate a standard analog video output (RS-170 protocol). The Hitachi and Sony cameras have a signal-to-noise ratio of 56 dB, which is equivalent to a binary value of

$$\frac{56\ \mathrm{dB}}{20}\cdot\frac{\ln 10}{\ln 2} = 9.3\ \mathrm{bit}\quad ,$$

therefore, 10-bit quantization is sufficient for the output signal. A higher resolution would only yield noise in least significant bits, given optimal use of the A/D converter's dynamic range. The 50 dB signal-to-noise ratio of the Pulnix camera converts to a binary value of 8.3 bit, which indicates a noise level twice as high as the Hitachi and Sony systems. Since the planned system is essentially a photometric ellipsometer operated close to the null condition, the detection and

quantification of weak signals is crucial for the performance of the device. Therefore, a high signal-to-noise ratio is required.

The analog RS-170 protocol reduces the chip resolution of 768 × 494 pixels to an effective 640 × 485 pixels for display on a standard video monitor. This reduction is implemented mainly to compensate for variations in the synchronization signals in the video output. We used the camera's pixel-synchronous output mode, because this mode has several advantages. One advantage is that full chip resolution can be utilized, because the pixel mode has higher synchronization accuracy than horizontal sync signals. Additionally, when reading the intensity distribution of a line from an RS-170 video signal alone, the data acquisition is only synchronized (by the H-sync signal) at the start and the end of the line. When reading the intensity values into memory at a constant rate, one has to assume that the clock does not vary in frequency, because this would lead to lateral displacement of the picture elements. When reading the video signal using the pixel clock for synchronization, the location of each pixel can be clearly identified, giving higher accuracy to spatially resolved measurements. ***We chose the Sony camera over the Hitachi camera because of its pixel clock output, which allowed us to perform the described pixel-synchronous acquisition.***

The Kodak Megaplus represented a novel type of camera for technical imaging applications. This camera incorporates arrays with more than 1024 × 1024 (1k × 1k) pixels and A/D conversion inside the camera, and interfaces with the frame grabber board using the digital RS-422 protocol. While the high resolution and digital interface makes these cameras favorable candidates for demanding imaging applications, their high price ($5000 - $15,000) would make the ellipsometric system very expensive.

For increasing the signal-to-noise ratio of a CCD-based system above the range of a 10-bit system, the camera generally has to be cooled. This would rule out the use of standard video cameras and complicate the selection of the video acquisition board. Therefore, in order to reduce the overall system cost, we decided to investigate the limits of a device based on standard components. ***The Sony XC-73 was therefore chosen for the system.***

2.6 Selection of Image Acquisition Board

For implementing pixel-synchronous image acquisition using 10-bit quantization of the intensity data, both the camera and the frame grabber board had to meet these requirements. A review of the

specifications of a number of frame grabber boards produced the following boards for consideration:

Table 2-4. Specifications of Commercially Available Frame Grabber Boards

Manufacturer	Type #	Type/On-Board Memory	A/D Quantization	Additional Features
Matrox	Corona	PCI, 4 MB	8 bit	color board, external pixel clock input
Matrox	Pulsar	PCI, 4 MB	8 or 10 bit	monochrome, external pixel clock input
Mutech	M-Vision 1000	PCI, 1 or 4 MB	8 or 10 bit	monochrome/color, external pixel clock input
Coreco	Ultra II	PCI, 1,2, or 4 MB	8 bit	monochrome / color board
Dipix	LPG-132	PCI, 1 MB	8 bit	monochrome, programmable preamp

All recent boards are designed for the peripheral component interconnect (PCI) bus, which offers independence of the specific computer platform and a high data throughput rate (up to 50 MB per second). Most of the cameras designed for color applications only have 8-bit A/D converters. The two additional bits of the 10-bit converter double the space required for storing the image, which can create problems for already large color images. The Matrox Corona, Coreco Ultra-II, and Dipix LPG-132 were therefore not capable of utilizing the full dynamic range given by the camera's signal-to-noise ratio. While both the Matrox Pulsar and the Mutech M-Vision 1000 offered 10-bit quantization and the possibility of pixel synchronous readout, ***we decided to choose the Mutech board, which was subsequently ordered.*** This board has a comprehensive selection of dynamic link libraries (DLLs) that can be implemented into our own image processing software to interface with the board functions.

2.7 Establishment of Theoretical Model for Ellipsometer Measurements

Jones calculus was used as the theoretical model to describe light passing through the ellipsometer. The Jones calculus uses vectors to represent the polarization state of fully polarized light, and transfer matrices to describe the effect of individual components on the polarization state of the light propagating through them [5].

A light beam can be described as an oscillating electrical field E and an oscillating magnetic field M, that are perpendicular to each other and to the direction of light propagation. The electric field of a monochromatic wave of angular frequency ω can be written as $E = E_0 \exp(i\omega t - ikz)$, where E_0 is a complex number. The real part of E describes the instantaneous electric field at a point z and a time t, and E_0 is the amplitude of the oscillating electric field.

If we consider monochromatic light propagating through an isotropic material in the z-direction in an xyz-coordinate system, E_0 lies in the xy-plane. Two perpendicular oscillating components are needed to describe the electrical field, one in the x-direction and one in the y-direction. If we observe the light at z = 0 looking into the beam, we can describe the light by a two component vector, known as the Jones vector:

$$\begin{pmatrix} E_{0,x} \\ E_{0,y} \end{pmatrix} \cdot \exp(i\omega t) \quad . \tag{2-1}$$

Usually, the time-dependent exponential term is omitted for the sake of shortness, but the time dependence of the field has to be taken into account when necessary. The polarization state of linearly polarized light at an angle θ to the x-axis is given by

$$\begin{pmatrix} E_0 \cos\theta \\ E_0 \sin\theta \end{pmatrix} \quad , \tag{2-2}$$

whereas the polarization state of (right-handed) circularly polarized light is given by

$$\begin{pmatrix} E_0 \\ i \cdot E_0 \end{pmatrix} \quad , \tag{2-3}$$

where i provides a 90° phase shift between the oscillating components of the electrical field. The Jones vector of elliptically polarized light, the most general case, is given by

$$\begin{pmatrix} E_x \\ E_y \end{pmatrix} = \begin{pmatrix} E_{x,r} + i \cdot E_{x,i} \\ E_{y,r} + i \cdot E_{y,i} \end{pmatrix} \quad , \tag{2-4}$$

where the indices r and i denote the real and the imaginary part of the field component, respectively.

In the Jones calculus, polarizing optical elements are represented by a 2×2 complex matrix called the Jones matrix. When light travels through a polarizing element, the change in polarization can be calculated by multiplying the Jones matrix of the respective element with the Jones vector of the incident light; the resulting Jones vector represents the polarization state of the light emerging from the element. The polarization variation through the ellipsometer can therefore be traced by successive application of the appropriate Jones matrices for the respective elements of the system.

The Jones matrix for a non-ideal polarizer with its transmission axis at an angle P to the x-axis is given by

$$\begin{pmatrix} \cos^2 P + X\sin^2 P & (1-X)\sin P\cos P \\ (1-X)\sin P\cos P & \sin^2 P + X\cos^2 P \end{pmatrix} , \tag{2-5}$$

with X denoting the extinction coefficient of the orthogonal polarization direction. With the quarter-wave plate at an angle Q to the x-axis being described by the following matrix:

$$\begin{pmatrix} \cos^2 Q - i\sin^2 Q & (1+i)\sin Q\cos Q \\ (1+i)\sin Q\cos Q & \sin^2 Q - i\cos^2 Q \end{pmatrix} , \tag{2-6}$$

the Jones vector for light falling onto the sample is described by

$$\begin{pmatrix} \cos Q[\cos(P-Q) + X\sin(P+Q)] + i\sin Q[\sin(P-Q) + X\cos(P+Q)] \\ \sin Q[\cos(P-Q) + X\sin(P+Q)] + i\cos Q[\sin(P-Q) + X\cos(P+Q)] \end{pmatrix} , \tag{2-7}$$

when unpolarized light is incident onto the first polarizer. The reflection from a sample surface with a single film on a substrate is described by the reflection matrix

$$\begin{pmatrix} \dfrac{r_{12_p} + r_{23_p}\exp(-2i\delta)}{1 + r_{12_p} r_{23_p}\exp(-2i\delta)} & 0 \\ 0 & \dfrac{r_{12_s} + r_{23_s}\exp(-2i\delta)}{1 + r_{12_s} r_{23_s}\exp(-2i\delta)} \end{pmatrix} , \tag{2-8}$$

where r_{12} and r_{23} denote the Fresnel reflection coefficients at the air-film and the film-substrate interface, and the indices p and s denote the polarization parallel and perpendicular to the plane of incidence, respectively. The variable δ describes the phase shift of the light when passing through the film. The Fresnel coefficients and δ are defined by the complex refractive indices of the

ambient environment, film and substrate, the film thickness, the angle of incidence, and the wavelength of the light.

After being reflected, the light passes through the analyzer, which is represented by a matrix mathematically identical to Eq. (2-5), and is detected by a photodiode or camera. The energy measured is determined by the square of the two components of the Stokes vector of the light emerging from the analyzer.

The set of expressions derived relates the relative intensity measured on the detector to the sample parameters and the azimuthal settings of the polarizing elements. A variety of programs were established to implement these formulas using the MatLab™ platform (MathWorks Inc., MA). With these programs, we were able to perform fits to the acquired measurement data sets, and visualize the output's dependence on parameter variations.

2.8 Establishment of Ellipsometer Test Samples

The performance of the system was tested utilizing purchased samples and samples fabricated in-house. Commercial ellipsometer check samples, which are routinely used for ellipsometer calibrations, can be used for checking the overall performance of the setup. These samples can be purchased in NIST-traceable qualities; for the Phase I project, however, they were prohibitively expensive ($2000-3000 per sample). We obtained calibration samples from Rudolph Technologies, one of the major manufacturers of ellipsometer systems, at a fraction of this price. Although these samples do not have full NIST-traceability, they are routinely used by Rudolph Technology's customers to recalibrate their ellipsometers; the specified layer thickness is guaranteed to within 3Å. We obtained silicon check samples with SiO_2 films ($n = 1.462$) of 115 and 435 Å thickness, and one with a Si_3N_4 film ($n = 2.006$) of 907 Å thickness. These check samples are useful for testing the setup as a null ellipsometer, but these films are significantly thicker than the monolayers that ultimately need to be measured. We therefore acquired a set of blank silicon wafers (Transition Technology International, Sunnyvale, CA), covered by a native oxide film of 1-2 nm thickness. These samples were used both for direct calibration and for depositing additional thin films. In order to obtain samples that are coated with a layer of a few angstroms thickness, and that have a surface pattern which can be recognized by the imaging setup, we decided to chemically coat monolayers onto a section of a silicon sample, and leave the other section of the sample untreated. The principle is depicted in Figure 2-11.

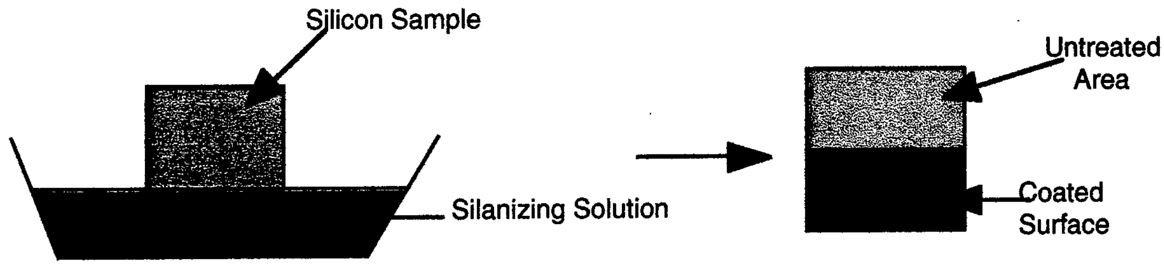

Figure 2-11
Coating principle for producing samples with a patterned surface layer of a few angstroms thickness.

For characterizing the system, monolayers of picometer thickness must be deposited on the surface of a substrate. Because of its unparalleled purity and extreme surface uniformity, a silicon wafer was chosen for depositing the monolayers. Preparing an amorphous monolayer of 1 to 10 Å is an extremely challenging task. The relative sizes of common materials are shown in Figure 2-12. From the figure it becomes evident that the substrate surface has to be extremely clean to attach angstrom thickness layers, as dust particles and other materials also can attach to the surface, forming structures much thicker than the created monolayer.

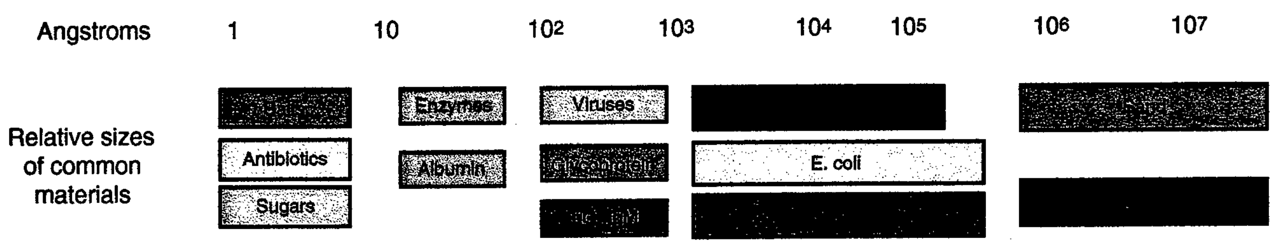

Figure 2-12
The relative sizes of various materials.

Silanization is a common procedure for attaching layers of silicon-containing organic compounds on glass surfaces. Silanes are available with one, two, or three reactive groups that can react with the glass surface. Accordingly, they are called mono-, di-, and tri-functional silanes. The silanization reaction process is shown in Figure 2-13. The silanization reaction is dependent on (a) the concentration of the silanizing reagent, (b) the solvent used for silanization, and (c) the chemical reaction time. Trifunctional silanes provide ten or more layers; bifunctional silanes

provide 3-10 layers; and monofunctional silanes provide a single monolayer. An extensive review of commercially available silanes was conducted; Table 2-5 shows the thicknesses of monolayers produced with different silanes. The approximate thickness of the layer was calculated using the bond-lengths from literature (see Table 2-6) [6].

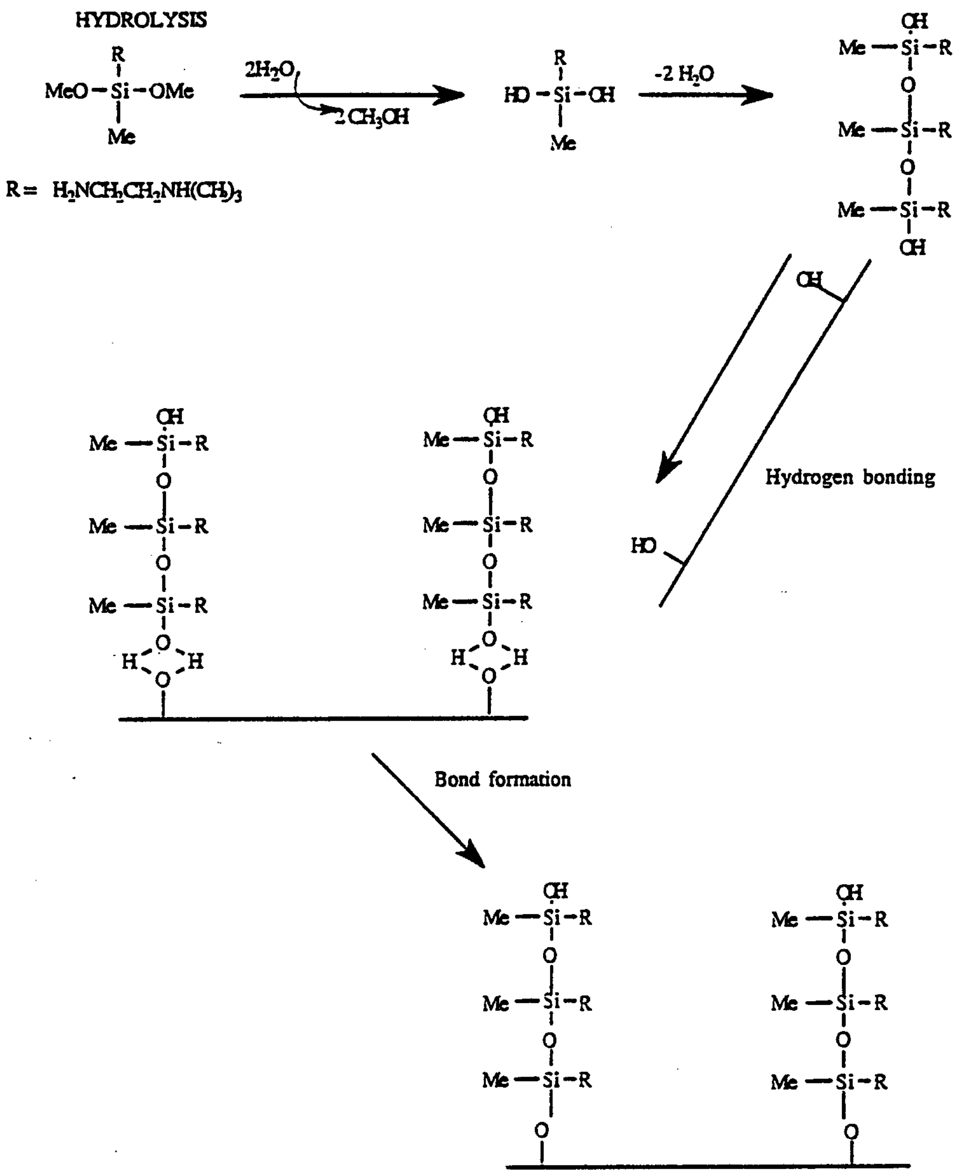

Figure 2-13
Silanization process for creating surface layers.

Table 2-5. Surface Layer Thicknesses for Various Silanes

Compound	Thickness of layer, pm
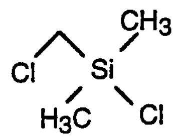 hloromethyldimethylchlorosilane	517
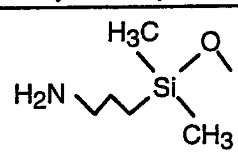 4-Aminobutyldimethylsiloxysilane	950
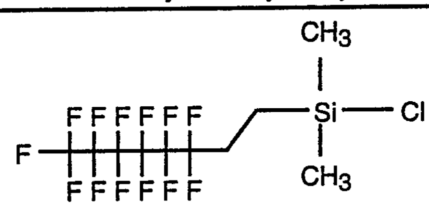 (Tridecafluoro-1,1,2,2-tetrahydrooctyl)-1-dimethylchlorosilane	1573
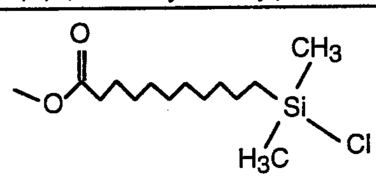 (10-Carbomethoxydecyl)dimethylchlorosilane	2315

Table 2-6. Bond Lengths for Different Molecule Combinations

Bond type	Bond length, pm
C–C	154.1
C–H	109.4
C=C	133.7
C–N	147.2
Si–O	153.5
C•Cl	176.7
O•O	148.0
C≡C	120.4
Si–Cl	201.9
C•O	142.6
C=O	121.5
Si–C	187.0

Deposition of silane monolayers on silicon wafer

Silicon wafers were washed in a strong oxidizing solution (H_2SO_4:H_2O_2 :: 2:1) for 2 hours followed by rinsing with deionized water. The cleaned silicon wafers were dried at room temperature with nitrogen and immediately used for silanization. Chlorosilane was added to anhydrous ethanol; the solution was made up to 5% (W/V). Chlorosilane reacts with ethanol to produce an alkoxy silane and hydrochloric acid. Progress of this reaction was observed by the halt of HCl evolution. The solution was warmed mildly to complete the reaction. Part of the HCl reacts with alcohol to produce small quantities of alkyl halide and water. The water causes formation of silanes from alkoxy silanes (see Figure 2-14). The salines condense on the substrate. Treated substrates were cured at 110°C on a hotplate for about 10 minutes.

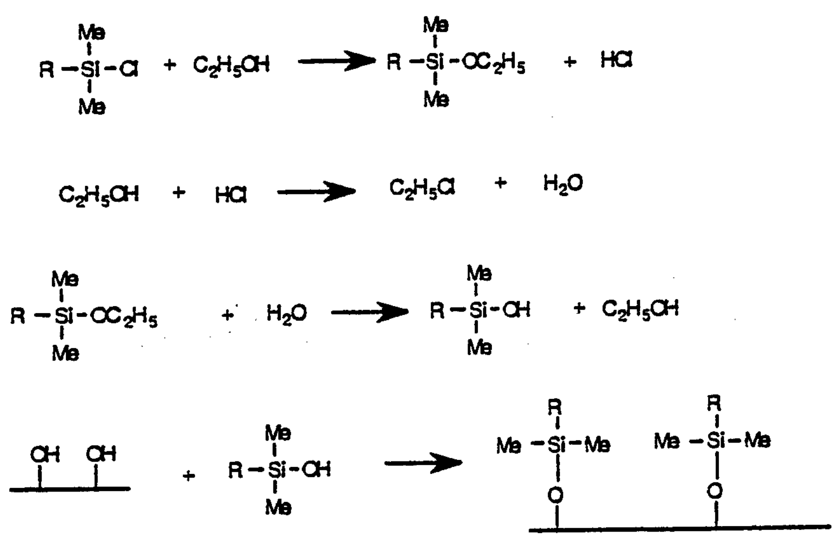

Figure 2-14
Silanization of silicon wafer using chlorosilanes.

Aminosilanes were attached on a cleaned wafer using an aqueous solution. In this case, a 95:5 ethanol water mixture containing 2% aminosilane was prepared. Cleaned silicon wafers were dipped in this solution for thirty minutes. The wafers were washed in ethanol to remove unattached silanes. The wafers were then ready to be tested on the ellipsometer setup.

2.9 Test Measurements and Data Interpretation

In the system's first test, the HeNe laser was used as a light source, and a blank silicon wafer was placed into the sample holder. The complex refractive index of silicon at the wavelength of the red HeNe laser ($\lambda = 632.8$ nm) is $n_{Si} = 3.875\text{-}0.018i$. The maximal polarizing effect due to the reflection from the sample occurs at the angle of incidence where the intensity reflection coefficient for the p-polarization R_p is at minimum (see Figure 2-15). While non-absorbing media show full extinction of R_p at the Brewster angle, sample absorption causes a finite value of R_p at the so-called quasi-Brewster angle, which is slightly shifted with respect to the Brewster angle. The data in Figure 2-15 was calculated using the formulas in Reference [7]. Based on these equations, the low absorption of silicon (k = 0.018) causes only a minute deviation of the quasi-Brewster angle ($\theta_{QB} = 75.5298°$) with respect to the Brewster angle ($\theta_B = 75.5297°$). The quasi-Brewster angle was subsequently used as the angle of incidence for the measurements.

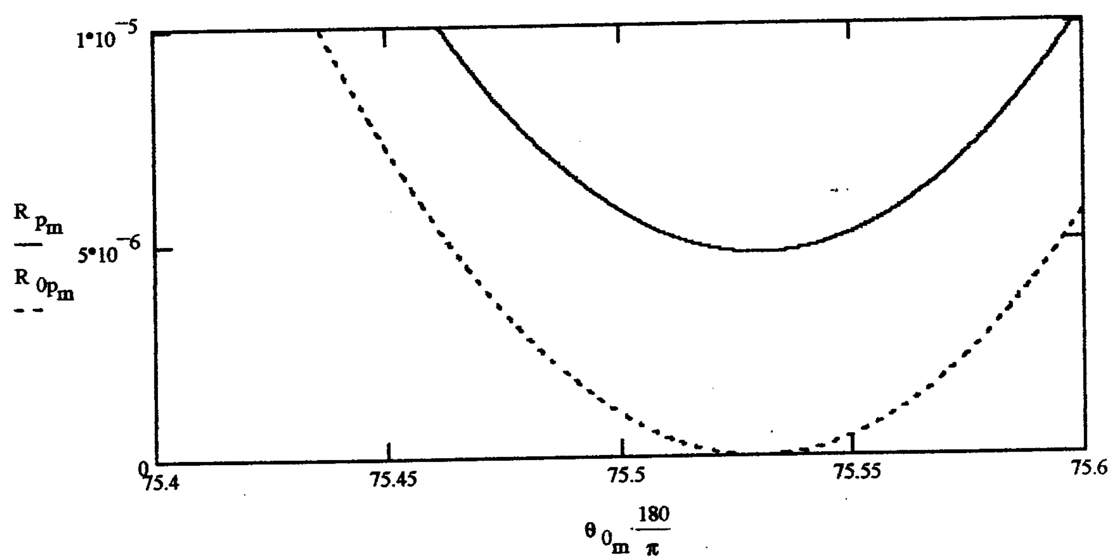

Figure 2-15
Intensity reflection coefficient R_p (for p-polarization) in dependence of the angle of incidence for silicon (full line) and for a material of equal refractive index with zero absorbance (dashed line).

The nulling angles revealed from the measurement were entered into the Matlab simulation programs that were established based on Formulas 2-1 to 2-8. Figure 2-16 shows the simulated relative intensity on the detector based on the angles and the refractive index of silicon. Since the minimum of this surface profile lies on the edge of the calculated area, it is obvious that a fit for the intensity minimum will always tend towards higher film thickness and lower film refractive index

until the given limits are reached; it is therefore not possible to determine *both* the film refractive index and thickness from the ellipsometer data for very thin films. This fundamental behavior of null ellipsometry is thoroughly discussed in ellipsometry textbooks [8]. However, when the refractive index of the film is held fixed, the intensity shows a clearly defined minimum; therefore the fit can very precisely determine the value of the film thickness, as indicated in Figure 2-17. The figure shows the intensity behavior for a film refractive index of n_f=1.457, revealing a film thickness of h_f = 1.699 nm, which is a reasonable value for native oxide on silicon.

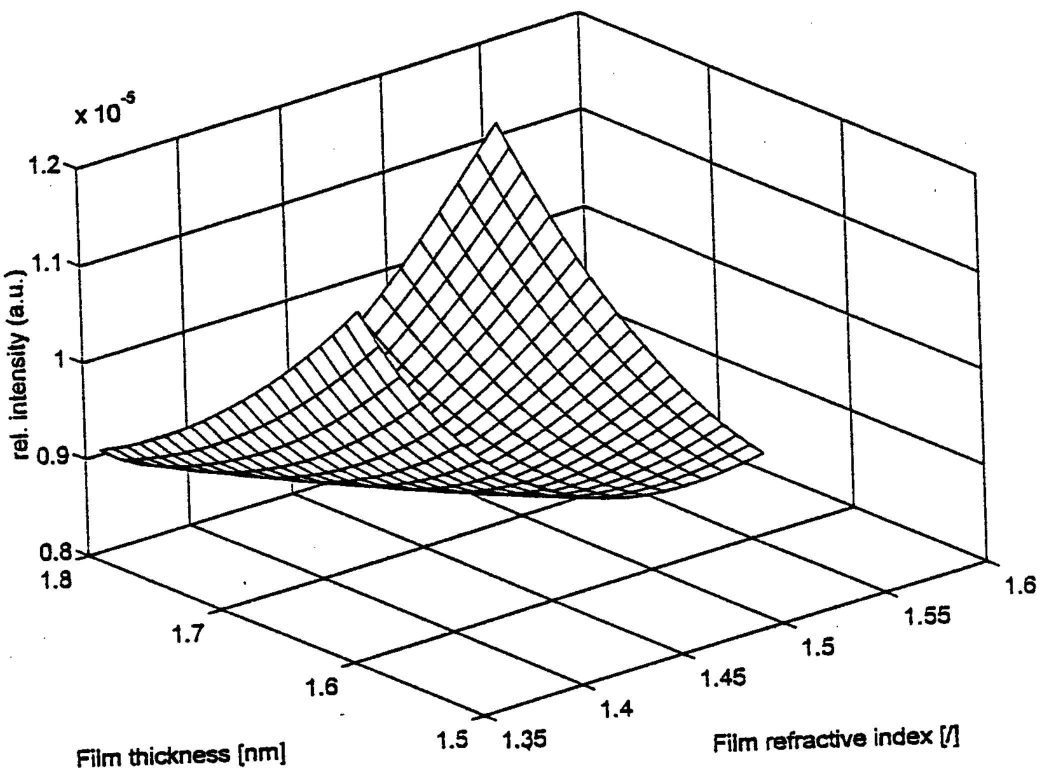

Figure 2-16
Simulated relative intensity on the detector in dependence of film parameters for a given set of measurement data from native oxide on a silicon wafer.

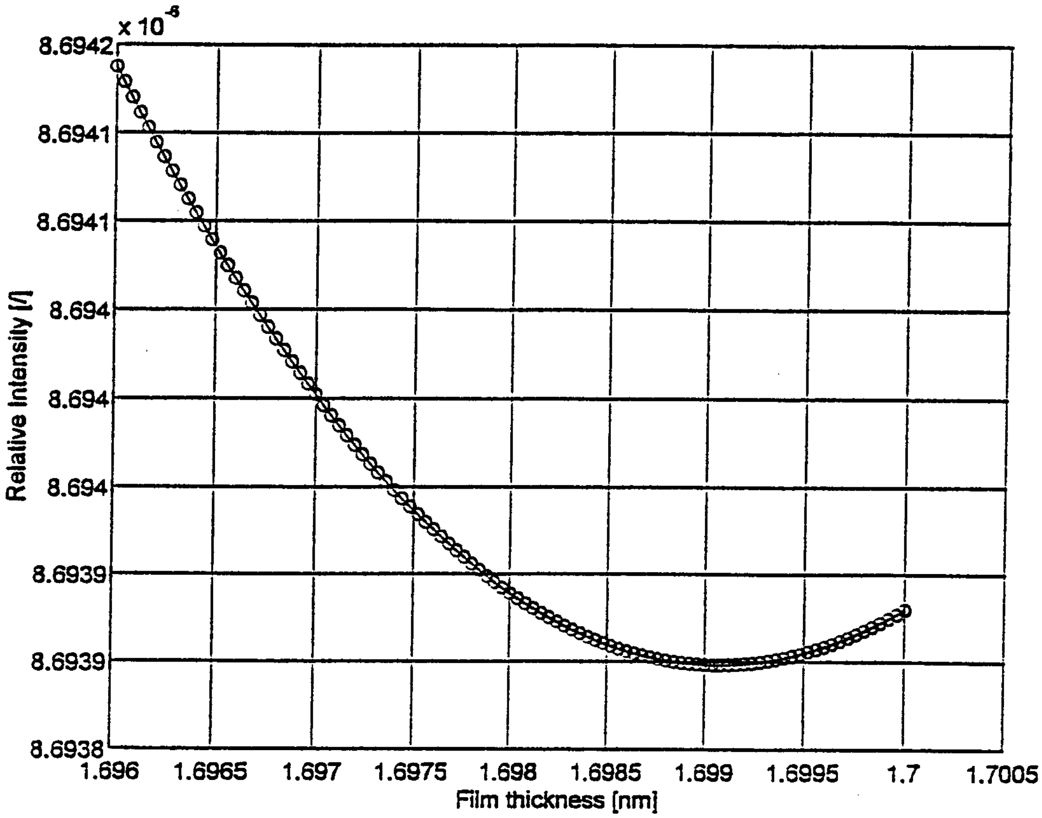

Figure 2-17
Simulated relative intensity on the detector in dependence of film thickness for a given set of measurement data from native oxide on a silicon wafer, film index fixed to $n_f = 1.457$.

We further investigated the effect of parameter variations on the simulation results. The data is presented in Table 2-7. The results indicated that the analyzer angle is the most critical parameter in thickness determination.

Table 2-7. Dependence of Film Thickness on Different Parameter Variations

	Parameter Variation	Thickness Variation	Sensitivity to Parameter
Angle of incidence	+0.1°	-0.0145 nm	-0.145 nm/°
Polarizer angle	+0.1°	-0.000571 nm	-0.00571 nm/°
Compensator angle	+0.1°	+0.00134 nm	+0.0134 nm/°
Analyzer angle	+0.1°	+0.17854 nm	+1.7854 nm/°
Film refractive index	$+1*10^{-3}$	-0.0017 nm	-0.0017 nm/10^{-3}
Substrate index	$+1*10^{-3}$	+0.000102 nm	$+0.000102$ nm/10^{-3}
Light wavelength	+0.1 nm	+0.000272 nm	+0.00272 nm/nm

As an additional test of the system, one of the ellipsometer test samples was characterized. The simulated intensity behavior based on the determined parameters is depicted in Figure 2-18. This figure again illustrates that the film refractive index cannot be determined by finding the intensity minimum in the calculated data. The POC system, however, can determine film thickness using the refractive index given by the manufacturer ($n_f = 1.462$). From our experimental results, the intensity with respect to the film thickness has a minimum at 43.6 nm (see Figure 2-19). The film thickness specified by the manufacturer is 43.8 nm +/- 0.3 nm. Therefore, ***the POC system correctly measured the thickness of the commercial test sample.***

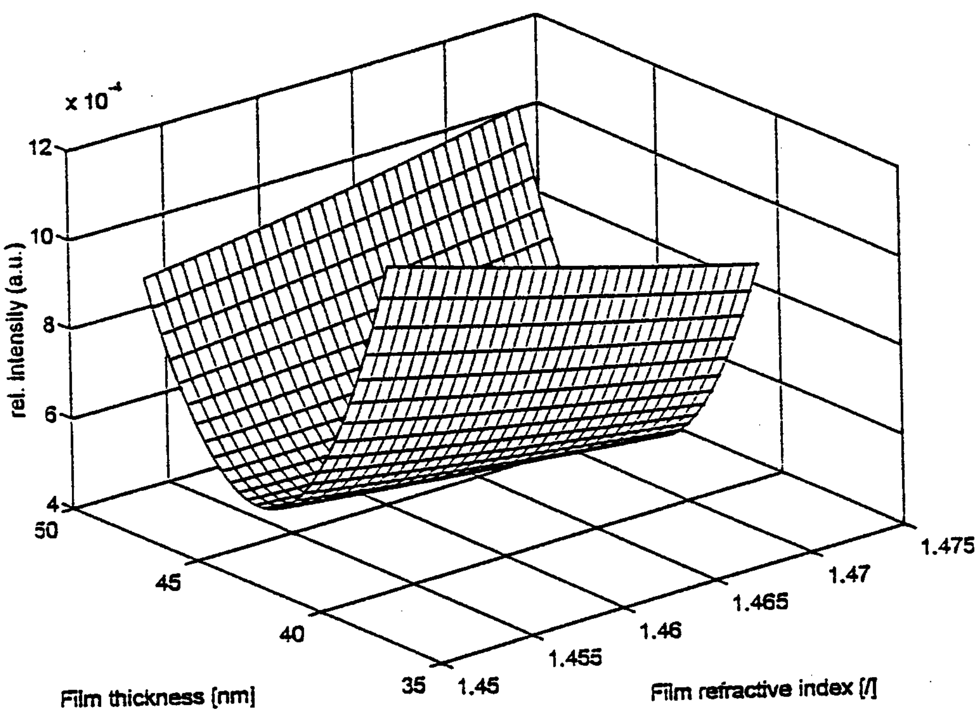

Figure 2-18
Simulated relative intensity on the detector in dependence of film parameters for a given set of measurement data from an ellipsometer test sample.

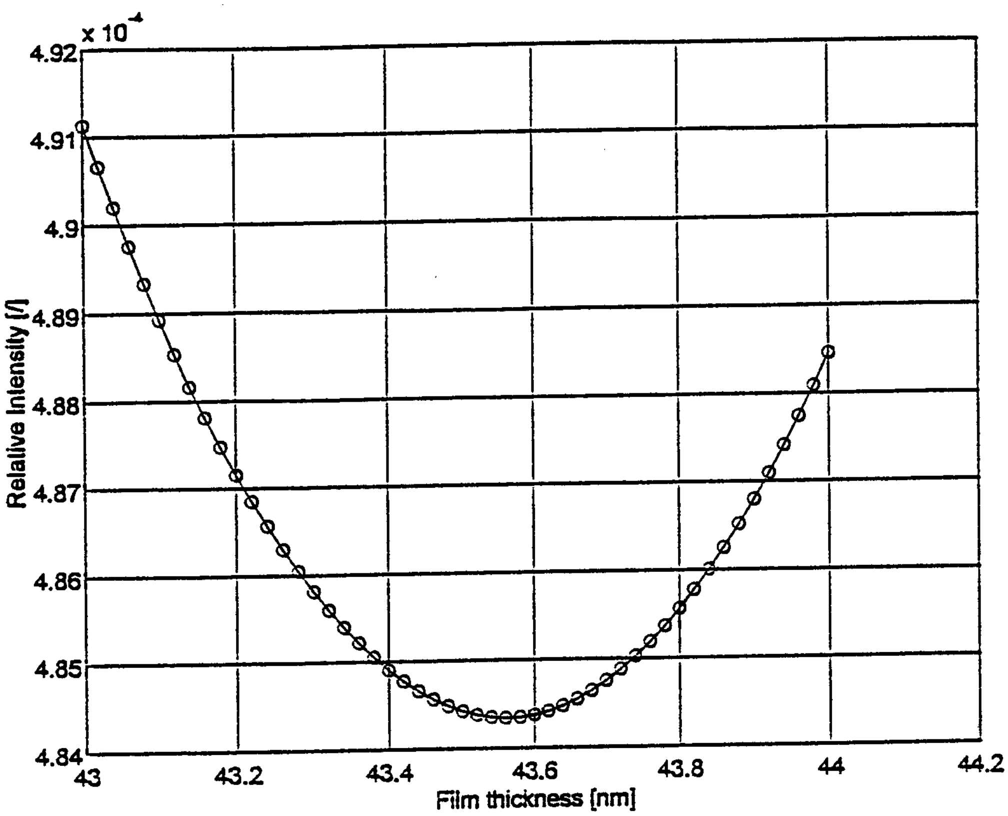

Figure 2-19
Simulated relative intensity on the detector in dependence of film thickness for a given set of measurement data from an ellipsometer test sample, with refractive index n=1.462.

3.0 CONCLUSION

Existing systems for film thickness analysis inside a vacuum reaction chamber do not meet the requirements for monitoring the growth of amorphous monolayers, partly due to their limited thickness resolution, and partly due to the lack of systems yielding the entire surface relief for monitoring coating uniformity. The technique investigated in this project offers the possibility of optically measuring film thickness inside a reaction chamber without interfering with the coating process. Using a single video frame from an imaging system, the film thickness is determined at more than 300,000 points (equivalent to the number of camera pixels), which is in sharp contrast to other concepts. The fast measurement speed allows the film growth to be monitored in parallel over the entire sample surface.

The foregoing sections clearly demonstrate that the proposed technique for an imaging ellipsometer for the detection of amorphous monolayers is feasible.

The optical system has been established and tested, and the system's functionality was demonstrated both on commercial test substrates and on specifically fabricated test samples with patterned amorphous films. Even without the multi-spectral extension of the system, which will be added in Phase II of the project, extremely thin films were detected, measured, and mapped. The software for evaluating the film parameters from the optical measurement and for predicting the ellipsometer system behavior has been established and successfully tested. Thus all the necessary components are available for the realization of a prototype film processing monitor (with monolayer sensitivity) that can be operated in a coating chamber.

4.0 REFERENCES

1. Micro Photonics Inc., Product Information on RAS 50 Surface Monitoring System, 1997.
2. R.E. Kirby, D. Wherry and M. Madden, "Oxygen Detection in Thin Silicon Dioxide Layers by Low-Energy X-Ray Fluorescence Spectrometry," *Journal of Vacuum Science & Technology A*, Vol. 11, No. 5, pp. 2687-2693, 1993.
3. G. Jin, R. Janson, and H. Arwin, "Imaging Ellipsometry Revisited: Developments for Visualization of Thin Transparent Layers on Silicon Substrates," *Review of Scientific Instruments*, Vol. 67, No. 8, pp. 2930-2936, 1996.
4. *Oriel Light Source Catalog II,* Oriel Corporation, Stratford, CT, 1994.
5. R.M.A. Azzam and N.M. Bashara, *Ellipsometry and Polarized Light*, Elsevier Science B.V., Amsterdam, ISBN 0-444-87016-4, 1987.
6. J.A. Dean, *Lange's Handbook of Chemistry,* 14th Edition, McGraw-Hill, Inc., NY, NY, 1992.
7. Jean M. Benett, "Polarization," in: *Handbook of Optics*, M. Bass, Ed., McGraw-Hill Inc., New York, pp. 5.7-5.12, 1995.
8. H.G. Tompkins, *A User's Guide to Ellipsometry*, Academic Press, Inc., San Diego, ISBN 0-12-693950-0, 1993.

REPORT DOCUMENTATION PAGE	Form Approved OMB NO. 0704-0188

1. AGENCY USE ONLY (Leave Blank)	2. REPORT DATE 5/31/98	3. REPORT TYPE AND DATES COVERED Final, 12/01/97 - 05/31/98

4. TITLE AND SUBTITLE Multi-Spectral Imaging Ellipsometer for Fast, In-Situ Monitoring of Monolayer Film Deposition	5. FUNDING NUMBERS DAAG55-98-C-0024
6. AUTHOR(S) Lothar Kempen	
7. PERFORMING ORGANIZATION NAME(S) AND ADDRESS(ES) Physical Optics Corporation 2520 W. 237th Street Torrance, California 90505	8. PERFORMING ORGANIZATION REPORT NUMBER 3445
9. SPONSORING / MONITORING AGENCY NAME(S) AND ADDRESS(ES) U. S. Army Research Office P.O. Box 12211 Research Triangle Park, NC 27709-2211	10. SPONSORING / MONITORING AGENCY REPORT NUMBER ARO 37914.1-PH-SBI

11. SUPPLEMENTARY NOTES

The views, opinions and/or findings contained in this report are those of the author(s) and should not be construed as an official Department of the Army position, policy or decision, unless so designated by other documentation.

12 a. DISTRIBUTION / AVAILABILITY STATEMENT	12 b. DISTRIBUTION CODE
Distribution authorized to U.S. Government Agencies only; contains proprietary information.	

13. ABSTRACT (Maximum 200 words)

The goal of the Phase I project was to demonstrate the feasibility of mapping the thickness of amorphous layers in the monolayer thickness range using an imaging ellipsometer setup. The optical system has been established and tested, and the system's functionality was demonstrated both on commercial test substrates and on specifically fabricated test samples with patterned amorphous films. Even without the multi-spectral extension of the system, which will be added in Phase II of the project, extremely thin films were detected, measured, and mapped. The software for evaluating the film parameters from the optical measurement and for predicting the ellipsometer system behavior has been established and successfully tested. Thus all the necessary components are available for the realization of a prototype film processing monitor (with monolayer sensitivity) that can be operated in a coating chamber.

14. SUBJECT TERMS Imaging, Spectroscopic, Ellipsometer, Film Coating, Monolayer	15. NUMBER OF PAGES 39
	16. PRICE CODE

17. SECURITY CLASSIFICATION OR REPORT	18. SECURITY CLASSIFICATION ON THIS PAGE	19. SECURITY CLASSIFICATION OF ABSTRACT	20. LIMITATION OF ABSTRACT
UNCLASSIFIED	UNCLASSIFIED	UNCLASSIFIED	UL

NSN 7540-01-280-5500

Standard Form 298 (Rev.2-89)
Prescribed by ANSI Std. 239-18
298-102